

# Mercury's capture into the 3/2 spin-orbit resonance including the effect of core-mantle friction

Alexandre C. M. Correia<sup>a,b,\*</sup>, Jacques Laskar<sup>b</sup>

<sup>a</sup>*Departamento de Física, Universidade de Aveiro, Campus de Santiago, 3810-193 Aveiro, Portugal*

<sup>b</sup>*Astronomie et Systèmes Dynamiques, IMCCE-CNRS UMR8028, Observatoire de Paris, UPMC, 77 Av. Denfert-Rochereau, 75014 Paris, France*

---

## Abstract

The rotation of Mercury is presently captured in a 3/2 spin-orbit resonance with the orbital mean motion. The capture mechanism is well understood as the result of tidal interactions with the Sun combined with planetary perturbations (Goldreich and Peale, 1966; Correia and Laskar, 2004). However, it is now almost certain that Mercury has a liquid core (Margot et al., 2007) which should induce a contribution of viscous friction at the core-mantle boundary to the spin evolution. According to Peale and Boss (1977) this last effect greatly increases the chances of capture in all spin-orbit resonances, being 100% for the 2/1 resonance, and thus preventing the planet from evolving to the presently observed configuration. Here we show that for a given resonance, as the chaotic evolution of Mercury's orbit can drive its eccentricity to very low values during the planet's history, any previous capture can be destabilized whenever the eccentricity becomes lower than a critical value. In our numerical integrations of 1000 orbits of Mercury over 4 Gyr, the spin ends 99.8% of the time captured in a spin-orbit resonance, in particular in one of the following three configurations: 5/2 (22%), 2/1 (32%) and 3/2 (26%). Although the present 3/2 spin-orbit resonance is not the most probable outcome, we also show that the capture probability in this resonance can be increased up to 55% or 73%, if the eccentricity of Mercury in the past has descended below the critical values 0.025 or 0.005, respectively.

*Key words:* Mercury, spin dynamics, tides, core-mantle friction, resonance

---

## 1. Introduction

Mercury's present rotation is locked in a 3/2 spin-orbit resonance, with its spin axis nearly perpendicular to the orbital plane (Pettengill and Dyce, 1965). The stability of this rotation results from the solar torque on Mercury's quadrupolar moment of inertia, combined with an eccentric orbit: the axis of minimum moment of inertia is always aligned with the direction to the Sun when Mercury is at the perihelion of its orbit (Colombo, 1965; Goldreich and Peale, 1966; Counselman and Shapiro, 1970). The initial rotation of Mercury was presumably faster than today, but tidal dissipation along with core-mantle friction brought the planet rotation to the present configuration, where capture can occur. However, the exact mechanism on how this state initially arose is not completely understood.

In their seminal work, Goldreich and Peale (1966) have shown that since the tidal strength depends on the planet's rotation rate, it creates an asymmetry in the tidal potential that allows capture into spin-orbit resonances. They also computed the capture probability into these resonances for a single crossing, and found that for the present eccentricity value of Mercury ( $e = 0.206$ ), and unless one uses an unrealistic tidal model with constant torques (which cannot account for the observed damping of the planet's libration), the probability of capture

into the present 3/2 spin-orbit resonance is on the low side, at most about 7%, which remained somewhat unsatisfactory.

Goldreich and Peale (1967) nevertheless pointed out that the probability of capture could be greatly enhanced if a planet has a molten core. In 1974, the discovery of an intrinsic magnetic field by the Mariner 10 spacecraft (Ness et al., 1974), seemed to imply the existence of a conducting liquid core and consequently an increment in the capture probability in the 3/2 resonance. However, according to Goldreich and Peale (1967), this also increases the capture probability in all the previous resonances. Peale and Boss (1977) indeed remarked that only very specific values of the core viscosity allow to avoid the 2/1 resonance and permit the capture in the 3/2 configuration.

More recently, Correia and Laskar (2004) (hereafter denoted by Paper I) have shown that as the orbital eccentricity of Mercury is varying chaotically, from near zero to more than 0.45, the capture probability is substantially increased. Indeed, when the large eccentricity variation is factored into the capture, the rotation rate of the planet can be accelerated, and the 3/2 resonance could have been crossed many times in the past. Performing a statistical study of the past evolutions of Mercury's orbit, over 1000 cases, it was demonstrated that capture into the 3/2 spin-orbit resonant state is in fact, and without the need of specific core-mantle effect, the most probable final outcome of the planet's evolution, occurring about 55.4% of the time. In contrast, because the eccentricity can decrease to near zero, all resonances except the 1/1 become unstable, allowing the planet to escape from resonance. This mechanism suggests that in pres-

---

\*Corresponding author,

Email addresses: correia@ua.pt (Alexandre C. M. Correia)

ence of core-mantle friction the planet can escape to a previous capture in the 2/1 or higher order spin-orbit resonances.

The present paper continues the work started in Paper I. In addition to the effects of tides and planetary perturbations, we will consider here also the core-mantle friction effect as described by Goldreich and Peale (1967), since the presence of a liquid core inside Mercury is now confirmed by radar observations (Margot et al., 2007). In the next section we give the averaged equations of motion in a suitable form for simulations of the long-term variations of Mercury's spin, including the resonant motion, viscous tidal effects, core-mantle coupling and planetary perturbations. In section 3 we discuss the consequences of each effect into the spin evolution and evaluate the capture probabilities in resonance. Finally, in last section we perform some numerical simulations to illustrate the different effects described in section 3.

## 2. Equations of motion

We will adopt here a model for Mercury which is an extension of the model from Poincaré (1910) of a perfect incompressible and homogeneous liquid core with moments of inertia  $A_c = B_c < C_c$  inside an homogeneous rigid body with moments of inertia  $A_m \leq B_m < C_m$ , supported by the reference frame  $(\vec{i}, \vec{j}, \vec{k})$ , fixed with respect to the planet's figure. Tidal dissipation and core-mantle friction drive the obliquity close to zero (Yoder, 1997; Correia et al., 2003). Since we are only interested here in the study of the final stages of evolution (where capture in spin-orbit resonance may occur), we will neglect the effect of the small obliquity variations on the equations of motion. Moreover, since for a long-term study we are not interested in diurnal nutations, we can average over fast rotation angles and merge the axis of principal inertia and the axis of rotation (Boué and Laskar, 2006). Therefore, the mantle rotation rate is simply given by  $\omega = \dot{\theta} + \dot{\varphi}$ , where  $\theta$  is the rotation angle and  $\varphi$  the precession angle.

### 2.1. Precession torque

The gravitational potential  $\mathcal{V}$  generated at a generic point of the space  $\vec{r}$  is given by (e.g. Tisserand, 1891; Smart, 1953):

$$\mathcal{V}(\vec{r}) = -\frac{Gm}{r} + \frac{G(B-A)}{r^3} P_2(\vec{u}_r \cdot \vec{j}) + \frac{G(C-A)}{r^3} P_2(\vec{u}_r \cdot \vec{k}), \quad (1)$$

where terms in  $(R/r)^3$  were neglected.  $G$  is the gravitational constant,  $m$  the mass of Mercury,  $\vec{u}_r = \vec{r}/r$  and  $P_2(x) = (3x^2 - 1)/2$  is the Legendre polynomial of degree two. When interacting with the Sun's mass,  $m_\odot$ , the spin of Mercury will undergo important changes. The middle term in the above potential will be responsible for a libration in the spin, while the last term causes the spin axis  $\vec{k}$  to precess around  $\vec{K}$ , the normal to the orbit. Since we are only interested in the study of the long term motion, we will average the potential over the rotation angle  $\theta$  and the mean anomaly  $M$ , after expanding the

true anomaly  $v$  in series of the eccentricity  $e$  and mean anomaly. However, when the rotation rate  $\omega$  and the mean motion  $n = \dot{M}$  are close to resonance ( $\omega \approx pn$ , for a semi-integer<sup>1</sup> value  $p$ ), we must retain the terms with argument  $(2\theta - 2pM)$  in the expansion

$$\frac{\cos(2\theta - 2v)}{r^3} = \frac{1}{a^3} \sum_{p=-\infty}^{+\infty} H(p, e) \cos(2\theta - 2pM), \quad (2)$$

where  $a$  is the semi-major axis of the planet's orbit and the function  $H(p, e)$  is a power series in  $e$  (Tab. 1). The exact averaged contributions to the spin are given in a suitable form for our study by expression (15) in Correia (2006)<sup>2</sup>. For zero obliquity we have:

$$\frac{d\omega}{dt} = -\frac{\beta}{c_m} H(p, e) \sin 2(\theta + \varphi - pM - \varpi), \quad (3)$$

where  $\varpi$  is the longitude of the perihelion,  $c_m = C_m/C = 0.55$  (Margot et al., 2007), and

$$\beta = \frac{3Gm_\odot}{2a^3} \frac{B-A}{C} \approx \frac{3}{2} n^2 \frac{B-A}{C}. \quad (4)$$

The Mariner 10 flyby of Mercury provided information on the internal structure of the planet, though subject to some uncertainty. For the gravity field it has been measured  $J_2 = (6.0 \pm 2.0) \times 10^{-5}$  and  $C_{22} = (1.0 \pm 0.5) \times 10^{-5}$  (Anderson et al., 1987). Modeling the interior structure of Mercury, it has been estimated for the structure constant  $\xi = C/(mR^2) \approx 0.3359$  (Spohn et al., 2001). Thus, for the moments of inertia we compute  $(B-A)/C = 4C_{22}/\xi \approx 1.2 \times 10^{-4}$ .

### 2.2. Tidal torques

Tidal effects arise from differential and inelastic deformations of Mercury due to the gravitational effect of the Sun. Their contributions to the spin variations are based on a very general formulation of the tidal potential, initiated by George H. Darwin (1880). The distortion of the planet gives rise to a tidal potential,

$$\mathcal{V}^s(\vec{r}, \vec{r}') = -k_2 \frac{Gm_\odot}{R} \left(\frac{R}{r}\right)^3 \left(\frac{R}{r'}\right)^3 P_2(\vec{u}_r \cdot \vec{u}_{r'}) . \quad (5)$$

where  $R$  is the average radius of the planet and  $r'$  the radial distance from the planet's center to the Sun. In general, imperfect elasticity will cause the phase angle of  $\mathcal{V}^s$  to lag behind the perturbation (Kaula, 1964), because there is a time delay  $\Delta t$  between the perturbation of the Sun and the maximal deformation of Mercury. During that time, the planet rotates by an angle  $\omega \Delta t$ , while the Sun also changes its position. Assuming a constant time delay allows us to linearize the tidal potential and simplify the tidal equations (Mignard, 1979, 1980; Hut, 1981).

<sup>1</sup>We have retained the use of semi-integers for better comparison with previous results.

<sup>2</sup>There is a misprint in the sign of  $\phi$  in Correia (2006).

Table 1: Coefficients of  $H(p, e)$  to  $e^7$ . The exact expression of these coefficients is given by  $H(p, e) = \frac{1}{\pi} \int_0^\pi \left(\frac{a}{r}\right)^3 \exp(i 2\nu) \exp(i 2pM) dM$ .

$p$	$H(p, e)$						
1/1	1	-	$\frac{5}{2}e^2$	+	$\frac{13}{16}e^4$	-	$\frac{35}{288}e^6$
3/2	$\frac{7}{2}e$	-	$\frac{123}{16}e^3$	+	$\frac{489}{128}e^5$	-	$\frac{1763}{2048}e^7$
2/1		$\frac{17}{2}e^2$	-	$\frac{115}{6}e^4$	+	$\frac{601}{48}e^6$	
5/2			$\frac{845}{48}e^3$	-	$\frac{32525}{768}e^5$	+	$\frac{208225}{6144}e^7$
3/1				$\frac{533}{16}e^4$	-	$\frac{13827}{160}e^6$	
7/2					$\frac{228347}{3840}e^5$	-	$\frac{3071075}{18432}e^7$
4/1						$\frac{73369}{720}e^6$	
9/2							$\frac{12144273}{71680}e^7$

For zero obliquity, the averaged contributions to the spin are then given by:

$$\frac{d\omega}{dt} = -\frac{K}{c_m} \left[ \Omega(e) \frac{\omega}{n} - N(e) \right], \quad (6)$$

where

$$\Omega(e) = \frac{1 + 3e^2 + 3e^4/8}{(1 - e^2)^{9/2}}, \quad (7)$$

$$N(e) = \frac{1 + 15e^2/2 + 45e^4/8 + 5e^6/16}{(1 - e^2)^6}, \quad (8)$$

$$K = n^2 \frac{3k_2}{\xi Q} \left(\frac{m_\odot}{m}\right) \left(\frac{R}{a}\right)^3, \quad (9)$$

and  $Q^{-1} = n\Delta t$ . This tidal model is particularly adapted to describe the planets behavior in slow rotating regimes ( $\omega \sim n$ ), which is the case of Mercury during the spin-orbit resonance crossing. In the present work we will adopt  $k_2 = 0.4$  and  $Q = 50$ , which yields  $K = 2.2 \times 10^{-5} \text{ yr}^{-2}$ . This choice is somewhat arbitrary, but based on the parameter values of the other terrestrial planets (Goldreich and Soter, 1966).

### 2.3. Core-mantle friction effect

The Mariner 10 flyby of Mercury revealed the presence of an intrinsic magnetic field, which is most likely due to motions in a conducting fluid core (for a review see Ness, 1978). Subsequent observations made with Earth-based radar provided strong evidence that the mantle of Mercury is decoupled from a core that is at least partially molten (Margot et al., 2007).

If there is slippage between the liquid core and the mantle, a second source of dissipation of rotational energy results from friction occurring at the core-mantle boundary. Indeed, because of their different shapes and densities, the core and the mantle do not have the same dynamical ellipticity and the two parts tend to precess at different rates (Poincaré, 1910). This tendency is more or less counteracted by different interactions produced at their interface: the torque of non-radial inertial pressure forces of the mantle over the core provoked by the non-spherical shape of the interface; the torque of the viscous friction (or turbulent) between the core and the mantle; and the torque of the electromagnetic friction, caused by the interaction between electrical currents of the core and the bottom of the magnetized mantle. The two types of friction torques (viscous and electromagnetic) depend on the differential rotation between the core and the mantle and can be expressed by a single effective friction torque,  $\Upsilon$  (Mathews and Guo, 2005; Deleplace and Cardin, 2006):

$$\Upsilon = C_c \kappa \delta; \quad \delta = \omega - \omega_c, \quad (10)$$

where  $\kappa$  is an effective coupling parameter,  $\omega_c$  the core's rotation rate and  $c_c = C_c/C = 1 - c_m = 0.45$  (Margot et al., 2007). According to Mathews and Guo (2005) we may write  $\kappa \simeq 2.62 \sqrt{\nu\omega}/R_c$ , where  $R_c$  is the core radius and  $\nu$  is the effective kinematic viscosity of the core. Adopting  $R_c/R = 0.77 \pm 0.04$  (Spohn et al., 2001) and  $\nu = 10^{-6} \text{ m}^2 \text{ s}^{-1}$ , we compute for the 3/2 resonance:  $\kappa = 5 \times 10^{-5} \text{ yr}^{-1}$ . The uncertainty over  $\nu$  is very large, according to Lumb and Aldridge (1991) it can cover about 13 orders of magnitude. As in former studies on planetary evolution (Yoder, 1997; Correia and Laskar, 2001, 2003), we used the same value as the best estimated so far for the Earth (Gans, 1972; Poirier, 1988).

Another important consequence of core-mantle friction is to tilt the equator of the planet to the orbital plane, which results in a secular decrease of the obliquity (Rochester, 1976; Correia, 2006), reinforcing the previous assumption that the obliquity remains close to zero during the last evolutionary stages.

Since the core and the mantle are decoupled, we need a differential equation for each rotation rate, the coupling equation being given by the friction torque (Peale, 2005; Correia, 2006):

$$\frac{d\omega}{dt} = -\frac{c_c \kappa}{c_m} \delta \quad \text{and} \quad \frac{d\omega_c}{dt} = \kappa \delta. \quad (11)$$

#### 2.4. Planetary perturbations

When considering the perturbations of the other planets, the eccentricity of Mercury is no longer constant, but undergoes strong chaotic variations in time (Laskar, 1990, 1994, 2008). These variations can be modeled using the averaging of the equations for the motion of the Solar System, that have been compared to recent numerical integrations, with very good agreement (Laskar et al., 2004a,b). These equations are obtained by averaging the equations of motion over the fast angles that are the mean longitudes of the planets. The averaging of the equation of motion is obtained by expanding the perturbations of the Keplerian orbits in Fourier series of the angles, where the coefficients themselves are expanded in series of the eccentricities and inclinations. This averaging process was conducted in a very extensive way, up to second order with respect to the masses, and through degree five in eccentricity and inclination, leading to truncated secular equations of the Solar System of the form

$$\frac{dw}{dt} = i [\Gamma w + \Phi_3(w, \bar{w}) + \Phi_5(w, \bar{w})], \quad (12)$$

where  $w$  is the column vector  $(z_1, \dots, z_8, \zeta_1, \dots, \zeta_8)$ , with  $z_j = e_j \exp(i\varpi_j)$ ,  $\zeta_j = \sin(I_j/2) \exp(i\Omega_j)$  and  $\varpi$  and  $\Omega$ , respectively the longitude of the perihelion and node. The  $16 \times 16$  matrix  $\Gamma$  is the linear Lagrange-Laplace system, while  $\Phi_3(w, \bar{w})$  and  $\Phi_5(w, \bar{w})$  gather terms of degree 3 and 5 respectively.

The system of equations thus obtained contains some 150000 terms, but its main frequencies are now the precession frequencies of the orbits of the planets. The full system can thus be numerically integrated with a very large step-size of 250 years. Contributions due to the secular perturbation of the Moon and general relativity are also included (for more details and references see Laskar, 1990, 1996; Laskar et al., 2004a).

This secular system is then simplified and reduced to about 50000 terms, after neglecting terms of very small value (Laskar, 1994). Finally, a small correction of the terms appearing in  $\Gamma$  (Eq.12), after diagonalization, is performed in order to adjust the linear frequencies, in a similar way as it was done by Laskar (1990). The secular solutions are very close to the direct numerical integration La2004 (Laskar et al., 2004a,b) over about 35 Myr, the time over which the direct numerical solution itself is valid because of the imperfections of the model. It is thus legitimate to investigate the diffusion of the orbital motion of Mercury over long times using the secular equations.

Over several millions years, the eccentricity of Mercury presents significant variations (Fig.1) that need to be taken into account in the resonance capture process (Paper I).

### 3. Spin evolution and capture probabilities

The evolution of the spin for zero obliquity is completely described when we put together the contributions from the different effects presented in section 2:

$$\begin{cases} \dot{\omega} = P + T - \Upsilon/C_m, \\ \dot{\omega}_c = \Upsilon/C_c, \end{cases} \quad (13)$$

where  $P$  is the precession torques (Eq.3),  $T$  the tidal torque (Eq.6) and  $\Upsilon$  the friction torque (Eq.10). In order to better study the capture probabilities in spin-orbit resonances, we will adopt a change of variables that is valid around each resonance  $p$ :

$$\gamma = \theta + \varphi - pM - \varpi, \quad (14)$$

and thus,

$$\dot{\gamma} = \omega - pn - \dot{\varpi} \quad \text{and} \quad \ddot{\gamma} = \dot{\omega} - \ddot{\varpi}. \quad (15)$$

In absence of planetary perturbations, for a Keplerian orbit,  $\ddot{\varpi} = 0$  and thus  $\ddot{\gamma} = \dot{\omega}$ . Instead of the core rotation  $\omega_c$  we will also adopt the differential rotation  $\delta = \omega - \omega_c$  as variable. The above system of equations (13) becomes then:

$$\begin{cases} \ddot{\gamma} = P(\gamma) + T(\dot{\gamma}) - c_c \kappa_m \delta - \ddot{\varpi}, \\ \dot{\delta} = P(\gamma) + T(\dot{\gamma}) - \kappa_m \delta, \end{cases} \quad (16)$$

where  $\kappa_m = \kappa/c_m$ . In general, we like to express  $\ddot{\gamma}$  as the sum of the precession torque  $P(\gamma)$  and a global dissipative torque  $D(\dot{\gamma})$  such that

$$\ddot{\gamma} = -\beta_m \sin 2\gamma + D(\dot{\gamma}), \quad (17)$$

where

$$\beta_m = \frac{\beta}{c_m} H(p, e) \quad (18)$$

and

$$D(\dot{\gamma}) = -D_0 \left( V + \mu \frac{\dot{\gamma}}{n} \right), \quad (19)$$

$D_0$ ,  $V$  and  $\mu$  being ‘‘constant’’ quantities. Indeed, under this linearized form we are able to estimate the capture probabilities using a simple expression derived by Goldreich and Peale (1966):

$$P_{\text{cap}} = 2 \left[ 1 + \frac{\pi}{2} \frac{n}{\Delta\omega} \frac{V}{\mu} \right]^{-1}, \quad (20)$$

where  $\Delta\omega$  is the maximal amplitude of libration in resonance, i.e.,  $\Delta\omega = \sqrt{2\beta_m}$ .

### 3.1. Effect of tides

Let us consider first the simplified case where the spin of the planet is only subject to the precession and tidal torques (Goldreich and Peale, 1966). Thus, we may use expression (17) to express  $\dot{\gamma}$ , where  $D(\dot{\gamma})$  is given by expression (6):

$$D(\dot{\gamma}) = T = -\frac{K}{c_m} \Omega(e) \left[ p - E(e) + \frac{\dot{\gamma}}{n} \right], \quad (21)$$

with  $E(e) = N(e)/\Omega(e)$ . The limit solution of the rotation for a constant value of the eccentricity is obtained when  $D(\dot{\gamma}) = 0$ , that is, for  $\dot{\gamma}/n = E(e) - p \Leftrightarrow \omega/n = E(e)$ . If the planet encounters a spin-orbit resonance in the way to the equilibrium position, capture may occur with a probability computed from expression (20):

$$P_{\text{cap}} = 2 \left[ 1 + \frac{\pi}{2} \frac{n}{\Delta\omega} (p - E(e)) \right]^{-1}. \quad (22)$$

Using the present value of the eccentricity of Mercury and  $c_m = 1$  we compute for the  $p = 3/2$  resonance a probability of capture of about 7%, which is unsatisfactory given that this is the presently observed resonant state.

### 3.2. Effect of core-mantle friction

We now add the effect of core-mantle friction to the effects already considered in the previous section. In this case we must take into account the rotation of the core, and the complete rotation rate evolution is given by system (16) with  $\ddot{\omega} = 0$ .

The general solution for the differential rotation in system (16) is given by:

$$\delta(t) = \delta_0 e^{-\kappa_m t} + e^{-\kappa_m t} \int_{t_0}^t [P(\dot{\gamma}) + T(\dot{\gamma})] e^{\kappa_m t'} dt', \quad (23)$$

where  $\delta_0$  is the initial value of  $\delta(t)$  for  $t = t_0$ . In section 2.3 we estimate for the present rotation of Mercury  $1/\kappa_m \simeq 10^4$  yr, which can be seen as the time scale needed to damp the initial differential rotation  $\delta_0$  to zero. Thus, for  $t \gg 1/\kappa_m$  the evolution of the differential rotation is given only by the last term in expression (23). It also means that for time intervals  $\Delta t \ll 1/\kappa_m$ , we can write for  $t < t_0 + \Delta t$ :

$$\delta(t) \simeq \delta_0 + \int_{t_0}^t \dot{\gamma} dt', \quad (24)$$

that is,

$$\delta(t) \simeq \delta_0 + \dot{\gamma} - \dot{\gamma}_0 = \dot{\gamma} - \dot{\gamma}_{c_0}, \quad (25)$$

where  $\dot{\gamma}_{c_0} = \dot{\gamma}_0 - \delta_0 = \omega_{c_0} - pn$ , and  $\omega_{c_0}$  is the value of the core rotation for  $t = t_0$ . This approximation is very useful because we can express  $\dot{\gamma}$  by means of expression (17) with

$$\begin{aligned} D(\dot{\gamma}) &= -\frac{K}{c_m} \Omega(e) \left[ p - E(e) + \frac{\dot{\gamma}}{n} \right] - \frac{c_c \kappa}{c_m} (\dot{\gamma} - \dot{\gamma}_{c_0}) \\ &= -\frac{K}{c_m} \Omega(e) \left[ p - E(e) - \chi \frac{\dot{\gamma}_{c_0}}{n} + (1 + \chi) \frac{\dot{\gamma}}{n} \right], \quad (26) \end{aligned}$$

where  $\chi = c_c \kappa n / [K \Omega(e)]$ . It allows us easily to compute the capture probabilities using expression (20) provided that we are able to estimate correctly  $\dot{\gamma}_{c_0}$  just before the planet crosses the resonance:

$$P_{\text{cap}} = 2 \left[ 1 + \frac{\pi}{2} \frac{n}{\Delta\omega} \frac{p - E(e) - \chi \frac{\dot{\gamma}_{c_0}}{n}}{1 + \chi} \right]^{-1}. \quad (27)$$

According to expression (11) we have  $\omega_c = \kappa \delta$ . Since  $\kappa \ll \Delta\omega$ , the core is unable to follow the periodic variations in the mantle's rotation rate. Thus, only the secular variations on the mantle will be followed by the core and we may write:  $\omega_c = \bar{\omega} - \bar{\delta}$ , where  $\bar{\omega}$  is the averaged rotation of the mantle and

$$\bar{\delta} \simeq e^{-\kappa_m t} \int_{t_0}^t T e^{\kappa_m t'} dt' \simeq \frac{T}{\kappa_m}. \quad (28)$$

Just before crossing the  $p^{\text{th}}$  spin-orbit resonance we have  $\bar{\omega}_0 = pn + 2\Delta\omega/\pi$ , and thus

$$\begin{aligned} \dot{\gamma}_{c_0} &= \omega_{c_0} - pn = \bar{\omega}_0 - \bar{\delta} - pn \\ &= \frac{2}{\pi} \Delta\omega - \frac{T}{\kappa_m} \simeq \frac{2}{\pi} \Delta\omega + \frac{K \Omega(e)}{\kappa} [p - E(e)]. \quad (29) \end{aligned}$$

When using the present eccentricity of Mercury and the values of  $\kappa$  and  $K$  estimated in previous sections, we compute  $\chi = 19.5$ . Substituting this into expression (27) we obtain a probability of capture of 100% in the 3/2 spin-orbit resonance. However, as noticed by Peale and Boss (1977), if we compute the probability for the 2/1 resonance we also get 100%. Thus, either the planet started its rotation below the 2/1 resonance, which is unlikely, or there must be another mechanism to avoid capture in the 2/1 and higher order resonances.

### 3.3. Effect of planetary perturbations

The orbital eccentricity of Mercury undergoes important secular perturbations from the other planets (Fig.1) and its contribution needs to be taken into account. The mean value of the eccentricity is  $\bar{e} = 0.198$ , slightly lower than the present value  $e \simeq 0.206$ , but we also observe a wide range for the eccentricity variations, from nearly zero to more than 0.45 (Paper I, Laskar, 2008). Even if some of these episodes do not last for a long time, they will allow additional capture into and escape from spin-orbit resonances. Moreover, the capture probabilities are also modified for different eccentricities: for the same resonance we can have zero or 100% of captures depending on the eccentricity value (Fig.2). For all resonances, the capture probability is 100% whenever the eccentricity is close to the equilibrium value for the rotation rate,  $E(e) = N(e)/\Omega(e)$  (Eq.21), but it tends to decrease as the eccentricity moves away from this equilibrium value. If the eccentricity is too high (or too low if the spin is increasing from lower rotation rates) some resonances cannot be reached and the probability of capture suddenly drops to zero (Fig.2).

Table 2: Critical eccentricity  $e_c$  for the resonance  $p$ . If  $e < e_c$ , the resonance  $p$  becomes unstable, and the solution may escape the resonance (Paper I). The critical eccentricity  $e_c$  is obtained when  $\beta H(p, e) < K[\Omega(e)p - N(e)]$ .

$p$	$e_c$
5/1	0.211334
9/2	0.174269
4/1	0.135506
7/2	0.095959
3/1	0.057675
5/2	0.024877
2/1	0.004602
3/2	0.000026
1/1	–

For a non-constant eccentricity  $e(t)$ , the limit solution of the rotation rate when  $D(\dot{\gamma}) = 0$  (Eq.17) is no longer  $\omega/n = E(e)$ , but more generally:

$$\omega(t) = \frac{1}{g(t)} \int_0^t \frac{K}{c_m} \left[ N(e(\tau)) - \frac{c_c K}{K} \delta(\tau) \right] g(\tau) d\tau, \quad (30)$$

where

$$g(t) = \exp\left(\frac{K}{c_m n} \int_0^t \Omega(e(\tau)) d\tau\right). \quad (31)$$

The dissipation torques can thus drive the rotation rate several times across the same spin-orbit resonance, increasing the chances of capture.

Another important consequence of a non-constant eccentricity is that all resonances but the 1/1 may become unstable. Indeed, the amplitude of the libration torque depends on the coefficient  $H(p, e)$  (Eq.3), which goes to zero with the eccentricity, except for the 1/1 resonance (Tab.1). Whenever the amplitude of the libration restoration torque becomes smaller than the amplitude of the dissipation torque, equilibrium in the spin-orbit resonance can no longer be sustained and the resonance is destabilized. Critical eccentricities for each resonance are listed in Table 2, obtained when the torques become equivalent (Eqs.3,6):

$$\frac{\Omega(e)p - N(e)}{H(p, e)} = \frac{\beta}{K}. \quad (32)$$

#### 4. Numerical simulations

We will now use the dynamical equations established in section 2 to simulate the final evolution of Mercury’s spin by performing massive numerical integrations. The main goal is to illustrate the effects described in section 3, in particular the probabilities of capture and escape from spin-orbit resonances. Mercury geophysical models and parameters in use are those listed in section 2. We recall here the most uncertain values:  $k_2 = 0.4$ ,  $Q = 50$  and  $\nu = 10^{-6} \text{m}^2 \text{s}^{-1}$ .

Table 3: Capture probabilities in several spin-orbit resonances (in percentage). In the left panel (T only) we consider the effect of tides alone, while in the right panel (T + CMF) both tides and core-mantle friction effects are taken into account. The first column ( $P_{\text{cap}}$ ) refers to the theoretical estimation given by expression (20), while the next column (num.) refers to the estimation obtained running a numerical simulation with 2000 close initial conditions, differing by  $\pi/1000$  in the libration angle. Planetary perturbations are not considered and we used a constant eccentricity  $e = 0.206$ .

$p$	T only		T + CMF	
	$P_{\text{cap}}$ (%)	num. (%)	$P_{\text{cap}}$ (%)	num. (%)
5/1	–	–	1.6	0.3
9/2	–	–	3.1	1.3
4/1	0.1	–	5.9	4.8
7/2	0.1	0.1	11.4	10.9
3/1	0.3	0.4	22.6	22.8
5/2	0.7	1.4	46.6	46.2
2/1	1.8	1.7	100.0	100.0
3/2	7.7	7.2	100.0	100.0

##### 4.1. Simulations without planetary perturbations

Before considering the effect of planetary perturbations we can test numerically the theoretical estimates of the capture probability given by expressions (22) and (27). Since capture in resonance is a statistical process we need to perform many integrations with slightly different initial conditions. For that purpose we ran 2000 simulations using a fixed eccentricity ( $e = 0.206$ ), initial rotation period of 2 days, zero obliquity and different initial libration phase angles with step-size of  $\pi/1000$  rad. Results are listed in Table 3. We can see that there is a good agreement between the theoretical previsions and the numerical estimation of the probabilities. As discussed in sections 3.1 and 3.2 the probability of capture when considering only the effect of tides is very small ( $\sim 7\%$  for the 3/2 resonance), while it becomes very important when core-mantle friction is added (100% for the 3/2 resonance). They are also in conformity with those obtained in the previous studies by Goldreich and Peale (1967) and Peale and Boss (1977). As they all noticed, when the effect from core-mantle friction is considered, the probabilities of capture are greatly enhanced for all spin-orbit resonances. In particular, capture in the 2/1 resonance also becomes 100%, preventing a subsequent evolution to the 3/2 resonance.

##### 4.2. Inclusion of planetary perturbations

When planetary perturbations are taken into account, the eccentricity presents chaotic variations with many excursions to higher and lower values than today (Laskar, 1990, 1994, 2008, Paper I). It is then impossible to know its exact evolution at the time the planet first encountered the spin-orbit resonances. A statistical study with many different orbital solutions is the only possibility to get a global picture of the past evolution of the spin of Mercury. In Paper I we performed such a study by integrating 1000 orbits over 4 Gyr in the past starting with very close initial conditions. This statistical study was only made

possible by the use of the averaged equations for the motion of the Solar System (Laskar, 1990, 1994).

In figure 3 we show five examples of the eccentricity evolution through the 4.0 Gyr. We choose some cases illustrative of the chaotic behavior, where we can see that the eccentricity can be as small as zero, but it can also reach values as high as 0.5. In some cases the eccentricity can remain within [0.1, 0.3] throughout the evolution, while in other cases it can span the whole interval [0, 0.5] (Laskar, 2008).

Owing to the chaotic evolution, the density function of the 1000 solutions over 4 Gyr is a smooth function (Fig.4), well approximated by a Rice probability distribution (Laskar, 2008). The eccentricity excursions to higher values allow the planet to cross the 3/2 resonance several times, and thus increase the probability of capture. This behavior becomes very important if the evolution is driven by tidal friction alone. Even though the probability of capture in a single crossing of the 3/2 spin-orbit resonance is only around 7%, multiple crossings increase it up to 55% (Paper I).

#### 4.3. Planetary perturbations with core-mantle friction

In presence of an efficient core-mantle friction the multiple crossings of the 3/2 resonance are no longer needed, since the capture in this resonance after a single crossing is already 100% (Fig.2). Nevertheless, eccentricity excursions to lower values can destabilize the equilibrium in any spin-orbit resonance different from the 1/1 (Tab.2). This effect was already present when the core-mantle friction was not considered (Paper I), but with small influence on the results, while here it becomes of capital importance. Indeed, it may allow the evasion from previous captures in higher order resonances than the 3/2 and permit subsequent evolution to the present observed spin state.

In order to check this new scenario, we have performed a statistical study of the past evolutions of Mercury’s orbit, with the integration of the same 1000 orbits over 4 Gyr in the past used in Paper I. We now additionally include the effect of core-mantle friction as described by Goldreich and Peale (1967), i.e., we will consider the full dynamics of the spin governed by Eq.(13).

Assuming an initial rotation period of Mercury of 10 h, we estimated that the time needed to de-spin the planet to the slow rotations would be about 300 million years. We will then start our integrations already in the slow-rotation regime, with a rotation period of 10 days ( $\omega \simeq 8.8n$ ), zero obliquity and a starting time of  $-4$  Gyr, although these values are not critical. In Table 4 we show the amount of captures for each resonance at the end of the simulations (column “final”). We also list the resonances in which the spin was first captured before being destabilized (column “1<sup>st</sup>cap.”) and we recall the results obtained for a constant eccentricity ( $e = 0.206$ ) and in Paper I, with a model without core-mantle friction.

After running 1000 trajectories we observe that the spin of Mercury preferably chooses one of the three final configurations: 5/2, 2/1 or 3/2 (Tab.4). With 26% of captures, the present configuration no longer represents the most probable final outcome, as it was in absence of core-mantle friction (Paper I). However, it is still among the most probable scenarios, the alternatives receiving comparable amounts of captures (22% and

Table 4: Capture probabilities in several spin-orbit resonances (in percentage). We performed a statistical study of the past evolutions of Mercury’s spin, with the integration of 1000 orbits over 4 Gyr, a initial rotation period of 10 days and zero obliquity. In the “1<sup>st</sup>cap.” column we list the resonances in which the spin was first captured (before being destabilized). In the “final” column we list the results after the full 4 Gyr of simulations. For comparison we also list the results obtained with a constant eccentricity  $e = 0.206$  (“const.”) and the final results obtained in Paper I (“C&L04”), with a model without core-mantle friction.

$p$	number of captures			
	const. (%)	1 <sup>st</sup> cap. (%)	final (%)	C&L04 (%)
6/1	–	0.1	–	–
11/2	–	0.4	–	–
5/1	0.3	1.3	–	–
9/2	1.3	2.7	–	–
4/1	4.7	5.3	–	–
7/2	10.3	8.7	4.7	–
3/1	19.0	15.5	11.6	–
5/2	29.8	26.5	22.1	–
2/1	34.6	31.2	31.6	3.6
3/2	–	8.1	25.9	55.4
1/1	–	0.2	3.9	2.2
none	–	–	0.2	38.3

32% respectively for the 5/2 and the 2/1 resonances). The 5/2 and the 2/1 spin-orbit resonances benefit from the fact that the planet must cross them first. On the other hand, the 3/2 resonance is more stable and the chances of capture are higher when crossed.

Since the eccentricity of Mercury 4.0 Gyr ago can be around 0.4 (e.g. Fig.3), at the moment of the first encounter with the spin-orbit resonances, capture in resonances as high as the 6/1 can occur (Fig.2). Because the probability of capture is small and because there are not many orbital solutions reaching such high values for the eccentricity, we only count about 10% of captures in resonances above or equal to the 4/1 (Tab.4). Once captured, these equilibria can be maintained as long as the eccentricity remains above the respective critical values (Tab.2).

Contrary to the results predicted for a constant eccentricity (Tab.4), we also registered a few trajectories directly captured in the 3/2 resonance just after the first passage through the resonance area. When we used the present value of the eccentricity ( $e = 0.206$ ), the 3/2 resonance could not be attained because for that value capture probability in the 2/1 resonance is 100% (Fig.2). However, for eccentricity values lower than about 0.19, the probability of capture in this resonance decreases, as well as for higher order resonances. For instance, when the eccentricity is 0.09, capture in the 2/1 resonance drops to 50%. Thus, since the eccentricity of Mercury is varying, it may happen that about 4.0 Gyr ago its value was much lower than today and the spin managed to avoid all the spin-orbit resonances higher than the 3/2 and was directly captured in the present observed configuration. We estimate nevertheless that the probability for this scenario to occur is very low, only about 8% (Tab.4).

#### 4.4. Critical eccentricities

Over 4.0 Gyr of evolution the eccentricity has many chances of experiencing a period of very small values (e.g. Fig.3). Even when a period of low eccentricity does not last for a long time, a single passage of the eccentricity below a critical value (Tab.2) can be enough to destabilize the corresponding spin-orbit resonance.

All orbital solutions were generated starting from initial conditions close to the present values (see Laskar, 2008), and therefore converge to the same final evolution. The eccentricity behavior is thus identical for the last 50-60 Myr (Fig.1), before which the chaotic diffusion dominates (Fig.5). During the last 50 Myr the eccentricity certainly reached values lower than 0.13, thus the 4/1 and above spin-orbit resonances cannot represent a possible final outcome for Mercury ( $e_{4/1} \approx 0.136$ ). For the 7/2 and lower order spin-orbit resonances, capture until the present day is not forbidden by the last 50 Myr of Mercury's evolution, but depends on the true orbital evolution of the eccentricity (Fig.5). The higher is the critical eccentricity, the lower is the probability of remaining trapped, because more orbital solutions will come below this value.

In figure 6 we plot the cumulative distribution of the minimal eccentricities attained for each one of the 1000 orbital solutions that we used. We also mark with straight lines the critical values of the eccentricity for each spin-orbit resonance (Tab.2) and use dots to represent the amount of captures obtained numerically for spin-orbit resonances that are still stable below each critical value of the eccentricity. Since a large amount of the orbital solutions experience at least one episode with an eccentricity below 0.05 ( $\log_{10} e \approx -1.3$ ), about 84% of the final evolutions will end in the 5/2 spin-orbit resonance or lower (Tab.4). By comparing the eccentricity instability thresholds for each spin-orbit resonance with the amount of captures obtained numerically below that resonance we see that there is a good agreement, suggesting a strong correlation between the orbital evolution of the eccentricity and the percentage of captures in each resonance. The reason why there is not full agreement between the two is because spin-orbit resonances below critical values of the eccentricity can also be attained by trajectories that escaped capture in higher order resonances, that is, they can be attained even if the eccentricity is never below the critical value for that resonance (Fig.2).

When comparing the results after 4.0 Gyr with those after the first capture, we verify that the 5/2 resonance (and above) lose a significant amount of previously captured solutions. The amount of orbits captured in the 2/1 resonance remains roughly the same, because the number of trajectories quitting this resonance is more or less compensated by the incoming trajectories from higher order resonances. The 3/2 is the real winner of this transition process, as the amount of trajectories that end in this last configuration is about 4 times larger than it was initially. An identical scenario was already observed in Paper I, except that only a few captures occurred in spin-orbit resonances higher than the 2/1 and they were all subsequently destabilized (Tab.4).

As in Paper I, we also noticed about 4% of the trajectories captured in the 1/1 spin-orbit resonance (Tab.4). Since the probability of capture in the 3/2 spin-orbit resonance is almost 100%

even for very low values of the eccentricity (Fig.2), the major possibility of evolving into the 1/1 resonance is by destabilizing the 3/2. This becomes a possibility if the eccentricity is almost zero, that is, for  $e < 3 \times 10^{-5}$  (Tab.2).

#### 4.5. Different scenarios of evolution

The critical eccentricity needed to destabilize the 2/1 spin-orbit resonance is  $e_{2/1} \approx 0.0046$  (Tab.2). Whenever the orbital eccentricity is below this value, the spin will then evolve towards the 3/2 resonance or below (Fig.7). However, this is not the only possibility of achieving this last configuration if the planet was first captured in a higher-order resonance. Indeed, as discussed for the 1<sup>st</sup> capture column (Tab.4), if the eccentricity is lower than 0.19 at the time the planet crosses the 2/1 resonance (Fig.2), the chances of capture are lower than 100%, opening some space for subsequent evolution to the 3/2 resonance. For instance, for a previous capture in the 5/2 resonance, an eccentricity of  $e_{5/2} \approx 0.025$  will destabilize it and produce a capture probability of only 14.4% in the 2/1 resonance, i.e., when the 5/2 resonance is destabilized there is about 85% of chance of ending in the 3/2 present configuration (Fig.7).

In order to exemplify the multitude of possible evolutionary scenarios, we performed another kind of experiment. Adopting a particular orbital solution, which presents a gradual decrease in the eccentricity (Fig.3a), we integrated close initial conditions for the spin. Since for this orbital solution the eccentricity is high at the time of the first encounter, there is a great chance of capturing the spin in a spin-orbit resonance with  $p > 5/2$ . In figure 7 we plot the behavior of four trajectories, each one initially captured in a different spin-orbit resonance, when the eccentricity approaches a zone of very low values. As expected, the spin-orbit resonances are sequentially abandoned as the eccentricity assumes small values. In particular, we observe that the resonances are quit immediately after the eccentricity is below the critical values listed in Table 2. After being destabilized, the spin can evolve directly to the present 3/2 configuration, or can be trapped in an intermediate spin-orbit resonance. In this example, the eccentricity become lower than  $e_{2/1} \approx 0.0046$  around  $-1.79$  Gyr and captures in the 2/1 resonance become destabilized after that date.

We purposely plot one situation, where the spin does not end in the 3/2 resonance, however. In this case, at the moment the eccentricity becomes lower than  $e_{2/1}$ , the spin is still captured in the 5/2 resonance. This resonance logically becomes destabilized and the rotation rate decreases. Nevertheless, at the moment the spin encounters the 2/1 resonance the eccentricity is again higher than  $e_{2/1}$ , and therefore there is a chance of capture in this resonance, preventing a subsequent evolution toward the 3/2 state (Fig.7).

#### 4.6. Constraints on the orbital evolution

We have seen in previous sections that there is an important correlation between the minimal eccentricity attained by Mercury through its orbital evolution and the probability of capture in a given resonance (Fig.6). The lower is the minimal eccentricity, the higher is the probability of achieving a low order



Table 5: Capture probabilities in spin-orbit resonances (in percentage), when the eccentricity descends below a given critical value (Tab.2).

$p$	$e_{3/2}$	$e_{2/1}$	$e_{5/2}$	$e_{3/1}$	$e_{7/2}$	$e_{4/1}$
7/2	–	–	1.2	2.6	3.8	4.7
3/1	–	2.0	4.2	7.2	10.7	11.6
5/2	–	3.2	5.2	16.0	20.7	22.1
2/1	3.1	5.4	23.9	30.5	32.6	31.6
3/2	25.0	73.2	55.1	37.2	27.7	25.9
1/1	68.8	15.4	9.7	6.1	4.2	3.9
none	3.1	0.7	0.5	0.3	0.2	0.2

spin-orbit resonance. In particular, each time the eccentricity descends below a given critical value for a spin-orbit resonance (Tab.2), the spin will evolve into a lower resonance.

Since we know the distribution of the minimal eccentricities (Fig.6), we can estimate the probability of ending in a specific spin-orbit resonance given the value of the minimal eccentricity of a considered orbit,  $P_{\text{cap}/e_c}$ . For that purpose we eliminate all the trajectories for which the minimal eccentricity is above the critical value (Tab.2) and then count the number of captures in each resonance for the remaining orbital solutions. Results are listed in Table 5. While for an arbitrary orbital solution the probability of capture in the present 3/2 spin-orbit resonance is only 25.9%, this value rises to 55.1% if we assume that the eccentricity of Mercury was below  $e_{5/2} \approx 0.025$  at some time in the past, or even up to 73.2% if the eccentricity descends below  $e_{2/1} \approx 0.0046$ . Results for the critical eccentricity  $e_{4/1} \approx 0.136$  are the same as the global results shown in Table 4, because the eccentricity of Mercury was below that value in the most recent 50 Myr, where the chaotic behavior is not significant (Fig.5). Notice also that there are always a few captures left in resonances above the corresponding critical value. This can be explained by the same effect described in the last paragraph of section 4.5 and illustrated in figure 7.

Inversely, since we know that the rotation of Mercury is presently captured in the 3/2 spin-orbit resonance, we can estimate the probability for the eccentricity to have descended during its past evolution below a specific critical level,  $P_{e_c}$ . Using conditional probabilities, we have then

$$P_{e_c} = \frac{P_{\text{cap}/e_c} \times P_{\text{orb}}}{P_{\text{cap}}}, \quad (33)$$

where  $P_{\text{cap}/e_c}$  is the probability of ending in a specific spin-orbit resonance given the value of the minimal eccentricity (Tab.5),  $P_{\text{orb}}$  the probability for the eccentricity to reach that minimal eccentricity (Fig.6) and  $P_{\text{cap}}$  the global capture probability in the specific spin-orbit resonance (Tab.4). Results for the 3/2 spin-orbit resonance are given in Table 6. These probabilities for the orbital evolution of the eccentricity are the same as if we select only the evolutions that finished in the 3/2 spin-orbit resonance and then look at the minimal eccentricity distribution. From the above analysis we conclude that there is a strong probability that the eccentricity of Mercury reached very low values; in particular there is about a 77% chance that it de-

Table 6: Probability for the eccentricity of Mercury to have descended below a specific critical level ( $P_{e_c}$ ) given that its rotation is captured in the 3/2 spin-orbit resonance today. Results for each critical eccentricity  $e_c$  (Tab.2) are obtained from Eq.(33) with  $P_{\text{cap}} = 25.9\%$  (Tab.4).

$P$	$e_{3/2}$	$e_{2/1}$	$e_{5/2}$	$e_{3/1}$	$e_{7/2}$	$e_{4/1}$
$P_{\text{cap}/e_c}$	25.0	73.2	55.1	37.2	27.7	25.9
$P_{\text{orb}}$	3.2	27.1	40.3	64.5	99.7	100.0
$P_{e_c}$	3.1	76.6	85.7	92.6	98.8	100.0

scended below  $e_{2/1} \approx 0.0046$  (but only a 3% chance of going below  $e_{3/2} \approx 0.00003$ ).

## 5. Conclusions

Due to the increasing evidence of a molten core inside Mercury (Ness et al., 1974; Margot et al., 2007), viscous friction at the core-mantle boundary is expected and its consequences to the spin must be taken into account. An important consequence is a considerable increase in the probability of capture for all spin-orbit resonances; in particular, for the 2/1 and the 3/2 it can reach 100% (Peale and Boss, 1977). Since it is believed that Mercury's initial rotation was much faster than today, a destabilization mechanism is then required to allow the planet to escape from the 2/1 and higher order resonances and subsequently evolve to the present observed 3/2 configuration.

With the consideration of the chaotic evolution of the eccentricity of Mercury we show that such destabilization mechanism exists whenever the eccentricity becomes smaller than a critical value for each spin-orbit resonance (Tab.2). This mechanism was already described in Paper I, but becomes of capital importance when core-mantle friction is taken into account. There are two main possibilities to evolve into the 3/2 configuration:

- The eccentricity becomes lower than the critical value for the 2/1 spin-orbit resonance ( $e_{2/1} \approx 0.005$ ) and evolves into the 3/2.
- The eccentricity becomes lower than the critical value for a higher order resonance than the 2/1, and then crosses this resonance with an eccentricity lower than  $e < 0.19$ . This allows a non zero probability of escaping the 2/1 resonance, and subsequent evolution into the 3/2.

The other mechanism of capturing in the 3/2 resonance described in Paper I, consisted in a returning to the 3/2 spin-orbit resonance after an increase in the eccentricity. This effect is not as important when we take into account core-mantle friction, since the most part of the trajectories are captured in resonance after a single passage.

After running 1000 orbital solutions, starting from 4 Gyr in the past until they reached the present date, the spin of the planet was captured in a spin-orbit resonance 99.8% of the time. The main resonances to be filled and the respective probability were (Tab.4):

$$P_{5/2} = 22.1\%, \quad P_{2/1} = 31.6\%, \quad P_{3/2} = 25.9\%. \quad (34)$$

Although in this case the present configuration no longer represents the most probable final outcome, as it was in absence of core-mantle friction (Paper I), it is still among the most probable scenarios.

Moreover, if we assume that at some time in the past, the eccentricity of Mercury becomes lower than  $e_{5/2} \approx 0.025$  or  $e_{2/1} \approx 0.005$  respectively, the probability of reaching the 3/2 spin-orbit resonance rises to 55% and 73% respectively (Table 5). Given that Mercury is presently trapped in the 3/2 configuration, we can also estimate that the eccentricity of Mercury has known at least one period of very low eccentricity during its past evolution, with about 86% and 77% of chances of being below  $e_{5/2} \approx 0.025$  and  $e_{2/1} \approx 0.005$  respectively (Table 6).

The probability of capture in the 3/2 resonance can also be increased if the orbital eccentricity experiences more periods near zero. This can be achieved if we use direct integration of the Solar System instead of the averaged equations, because the true eccentricity is expected to undergo some additional small variations around the value obtained for the averaged equations (Laskar, 2008). Alternatively, the probability of capture in the 3/2 resonance can still be increased if we are able to increase the critical eccentricities that destabilize spin-orbit resonances (Tab.2). This can be achieved if the tidal dissipation is stronger ( $k_2 > 0.4$  and/or  $Q < 50$ ) or if  $C_{22} < 1.0 \times 10^{-5}$  (Eq.32).

Lower values for the core effective viscosity,  $\nu$ , will not change the critical eccentricities, but will decrease the amount of captures for all spin-orbit resonances. As a consequence, it becomes easier to escape from the capture in spin-orbit resonances, and all those trajectories that also escape the 3/2 resonance can be later trapped there when the eccentricity experiences a period with  $e > 0.325$  (Paper I). We then believe that the true scenario for the evolution of the spin of Mercury may be somewhere between the scenario described here, with an efficient core-mantle friction effect, and the scenario described in Paper I, for a total absence of core-mantle friction. In the future, different dissipative parameters and models could be tested as well as the effect of the obliquity, that was supposed to be zero in the present study.

## Acknowledgments

The authors thank S.J. Peale for discussions. This work was supported by the Fundação Calouste Gulbenkian (Portugal), Fundação para a Ciência e a Tecnologia (Portugal), and by PNP-CNRS (France).

## References

Anderson, J. D., Colombo, G., Espitio, P. B., Lau, E. L., Trager, G. B., Sep. 1987. The mass, gravity field, and ephemeris of Mercury. *Icarus* 71, 337–349.  
 Boué, G., Laskar, J., Dec. 2006. Precession of a planet with a satellite. *Icarus* 185, 312–330.  
 Colombo, G., 1965. Rotational Period of the Planet Mercury. *Nature* 208, 575–578.  
 Correia, A. C. M., Dec. 2006. The core-mantle friction effect on the secular spin evolution of terrestrial planets. *Earth Planet. Sci. Lett.* 252, 398–412.  
 Correia, A. C. M., Laskar, J., Jun. 2001. The four final rotation states of Venus. *Nature* 411, 767–770.

Correia, A. C. M., Laskar, J., May 2003. Long-term evolution of the spin of Venus II. Numerical simulations. *Icarus* 163, 24–45.  
 Correia, A. C. M., Laskar, J., Jun. 2004. Mercury’s capture into the 3/2 spin-orbit resonance as a result of its chaotic dynamics. *Nature* 429, 848–850.  
 Correia, A. C. M., Laskar, J., Néron de Surgy, O., May 2003. Long-term evolution of the spin of Venus I. Theory. *Icarus* 163, 1–23.  
 Counselman, C. C., Shapiro, I. I., 1970. Spin-Orbit resonance of Mercury. *Symposia Mathematica* 3, 121–169.  
 Darwin, G. H., 1880. On the secular change in the elements of a satellite revolving around a tidally distorted planet. *Philos. Trans. R. Soc. London* 171, 713–891.  
 Deleplace, B., Cardin, P., Nov. 2006. Viscomagnetic torque at the core mantle boundary. *Geophys. J. Int.* 167, 557–566.  
 Gans, R. F., 1972. Viscosity of the Earth’s core. *J. Geophys. Res.* 77, 360–366.  
 Goldreich, P., Peale, S., Aug. 1966. Spin-orbit coupling in the solar system. *Astron. J.* 71, 425–438.  
 Goldreich, P., Peale, S., Jun. 1967. Spin-orbit coupling in the solar system. II. The resonant rotation of Venus. *Astron. J.* 72, 662–668.  
 Goldreich, P., Soter, S., 1966. Q in the Solar System. *Icarus* 5, 375–389.  
 Hut, P., Jun. 1981. Tidal evolution in close binary systems. *Astron. Astrophys.* 99, 126–140.  
 Kaula, W. M., 1964. Tidal dissipation by solid friction and the resulting orbital evolution. *Rev. Geophys.* 2, 661–685.  
 Laskar, J., Dec. 1990. The chaotic motion of the solar system - A numerical estimate of the size of the chaotic zones. *Icarus* 88, 266–291.  
 Laskar, J., Jul. 1994. Large-scale chaos in the solar system. *Astron. Astrophys.* 287, L9–L12.  
 Laskar, J., 1996. Large Scale Chaos and Marginal Stability in the Solar System. *Celestial Mechanics and Dynamical Astronomy* 64, 115–162.  
 Laskar, J., Jul. 2008. Chaotic diffusion in the Solar System. *Icarus* 196, 1–15.  
 Laskar, J., Correia, A. C. M., Gastineau, M., Joutel, F., Levrard, B., Robutel, P., Aug. 2004a. Long term evolution and chaotic diffusion of the insolation quantities of Mars. *Icarus* 170, 343–364.  
 Laskar, J., Robutel, P., Joutel, F., Gastineau, M., Correia, A. C. M., Levrard, B., Dec. 2004b. A long-term numerical solution for the insolation quantities of the Earth. *Astron. Astrophys.* 428, 261–285.  
 Lumb, L. I., Aldridge, K. D., 1991. On viscosity estimates for the Earth’s fluid outer core-mantle coupling. *J. Geophys. Geoelectr.* 43, 93–110.  
 Margot, J. L., Peale, S. J., Jurgens, R. F., Slade, M. A., Holin, I. V., May 2007. Large Longitude Libration of Mercury Reveals a Molten Core. *Science* 316, 710–714.  
 Mathews, P. M., Guo, J. Y., Feb. 2005. Viscoelectromagnetic coupling in precession-nutation theory. *J. Geophys. Res. (Solid Earth)* 110, B02402–16.  
 Mignard, F., May 1979. The evolution of the lunar orbit revisited. I. *Moon and Planets* 20, 301–315.  
 Mignard, F., Oct. 1980. The evolution of the lunar orbit revisited. II. *Moon and Planets* 23, 185–201.  
 Ness, N. F., Mar. 1978. Mercury - Magnetic field and interior. *Space Science Reviews* 21, 527–553.  
 Ness, N. F., Behannon, K. W., Lepping, R. P., Whang, Y. C., Schatten, K. H., Jul. 1974. Magnetic field observations near Mercury: Preliminary results from Mariner 10. *Science* 185, 153–162.  
 Peale, S. J., Nov. 2005. The free precession and libration of Mercury. *Icarus* 178, 4–18.  
 Peale, S. J., Boss, A. P., Aug. 1977. Spin-orbit constraint on the viscosity of a Mercurian liquid core. *J. Geophys. Res.* 82, 743–749.  
 Pettengill, G. H., Dyce, R. B., 1965. A Radar Determination of the Rotation of the Planet Mercury. *Nature* 206, 1240.  
 Poincaré, H., 1910. Sur la précession des corps déformables. *Bull. Astron.* 27, 321–356.  
 Poirier, J. P., Jan. 1988. Transport properties of liquid metals and viscosity of the earth’s core. *Geophysical Journal* 92, 99–105.  
 Rochester, M. G., 1976. The secular decrease of obliquity due to dissipative core-mantle coupling. *Geophys. J.R.A.S.* 46, 109–126.  
 Smart, W. M., 1953. *Celestial Mechanics*. London, New York, Longmans, Green.  
 Spohn, T., Sohl, F., Wiczerkowski, K., Conzelmann, V., Dec. 2001. The interior structure of Mercury: what we know, what we expect from Bepi-Colombo. *Plan. Space Sci.* 49, 1561–1570.  
 Tisserand, F., 1891. *Traité de Mécanique Céleste (Tome II)*. Gauthier-Villars, Paris.

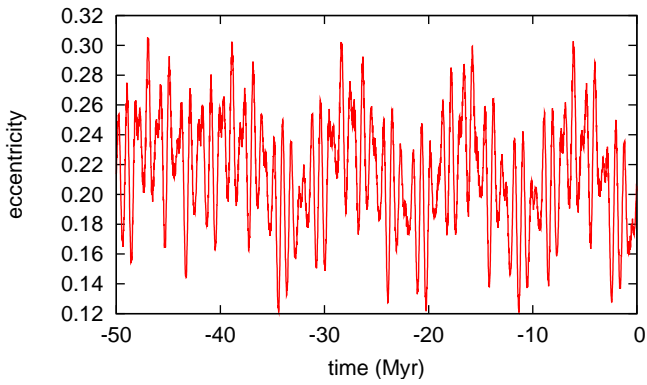


Figure 1: Evolution of Mercury's eccentricity over 50 Myr in the past (Laskar et al., 2004a,b).

Yoder, C. F., 1997. Venusian Spin Dynamics. In: Venus II: Geology, Geophysics, Atmosphere, and Solar Wind Environment. pp. 1087–1124.

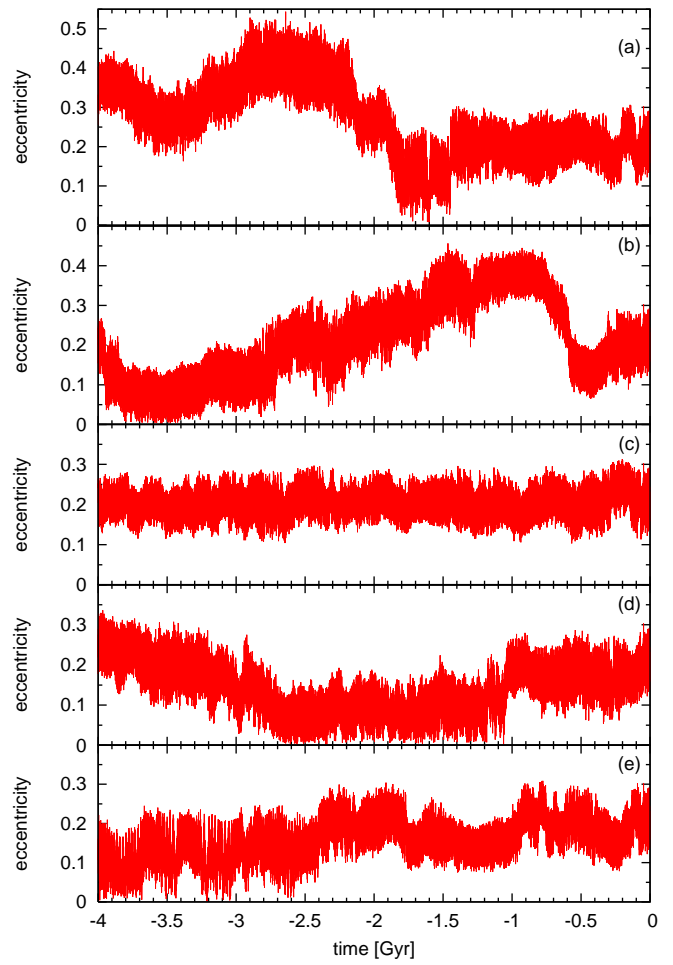


Figure 3: Some examples of the possible variations of the eccentricity of Mercury through the past 4.0 Gyr. The eccentricity can be as small as zero, but it can also reach values as high as 0.5. In some cases the eccentricity can remain within  $[0.1, 0.3]$  throughout the evolution, while in other cases it can span the whole interval  $[0, 0.5]$ . All these solutions converge to the known recent evolution of the planet's orbit (Fig.5).

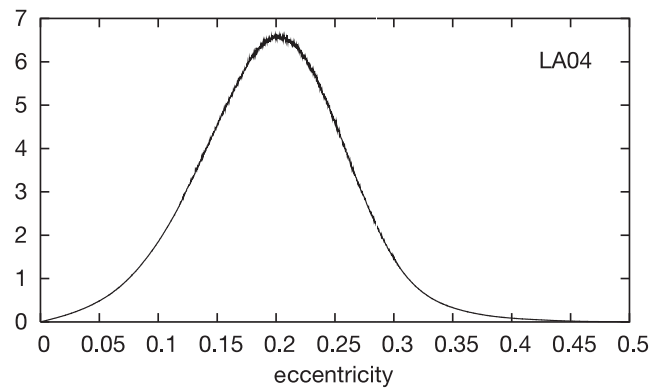


Figure 4: Probability density function of Mercury's eccentricity (Paper I). Values are computed over 4 Gyr for the numerical integration of the secular equations (Laskar et al., 2004a,b; Laskar, 2008) for 1000 close initial conditions (LA04). The mean value of the eccentricity is  $\bar{e} = 0.198$ .

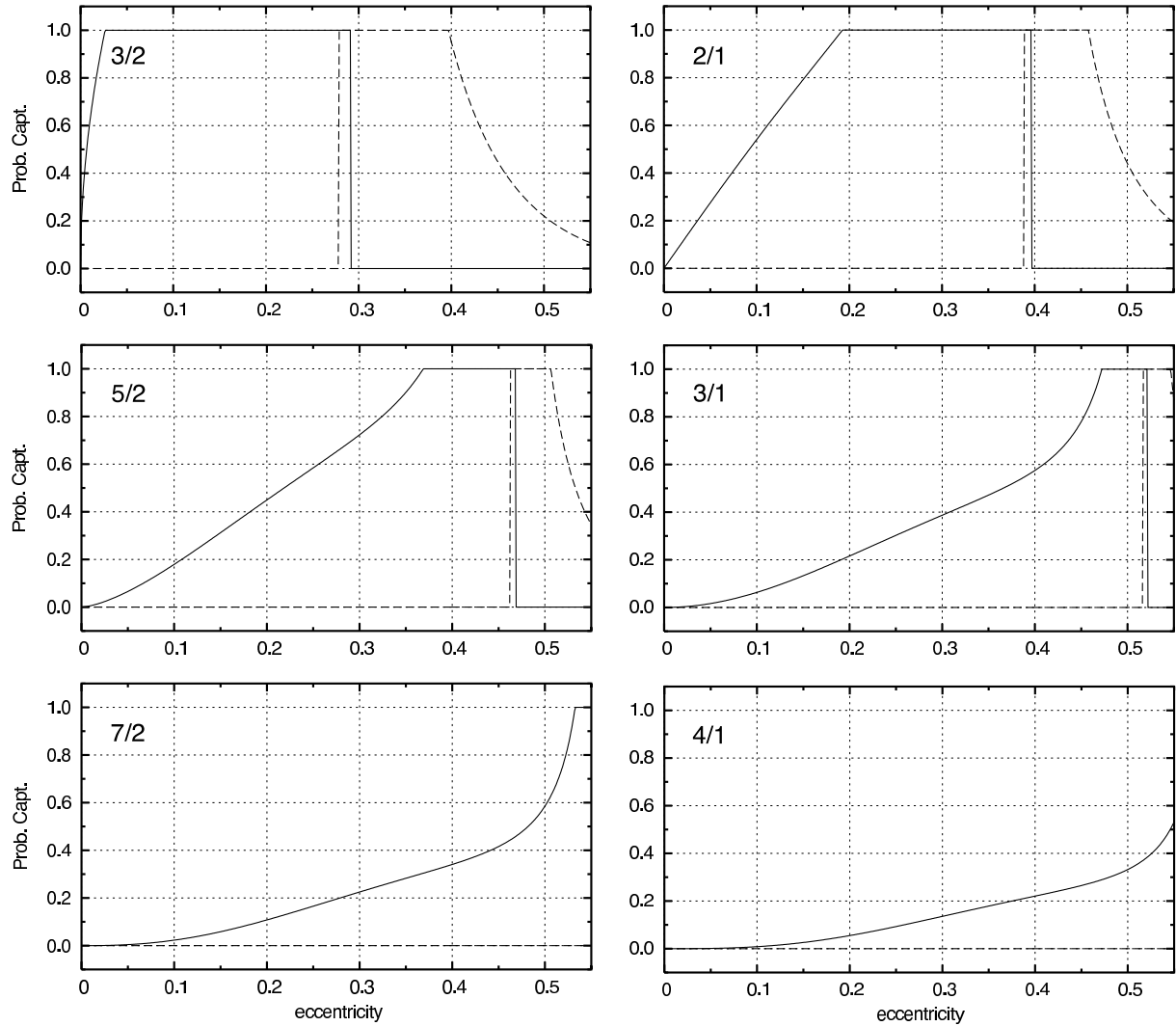


Figure 2: Probability of capture in some spin-orbit resonances for different values of the eccentricity, under the effect of tides and core-mantle friction (Eq.27). The dashed line corresponds to a planet increasing its spin from slower rotation rates, while the solid line corresponds to a planet de-spinning from faster rotation rates. For all resonances, capture probability is 100% whenever the eccentricity is close to the equilibrium value for the rotation rate,  $\omega/n = E(e)$  (Eq.21). It suddenly decays to zero when the equilibrium rotation rate falls outside the resonance width, i.e., the tidal evolution prevents the planet from crossing the resonance.

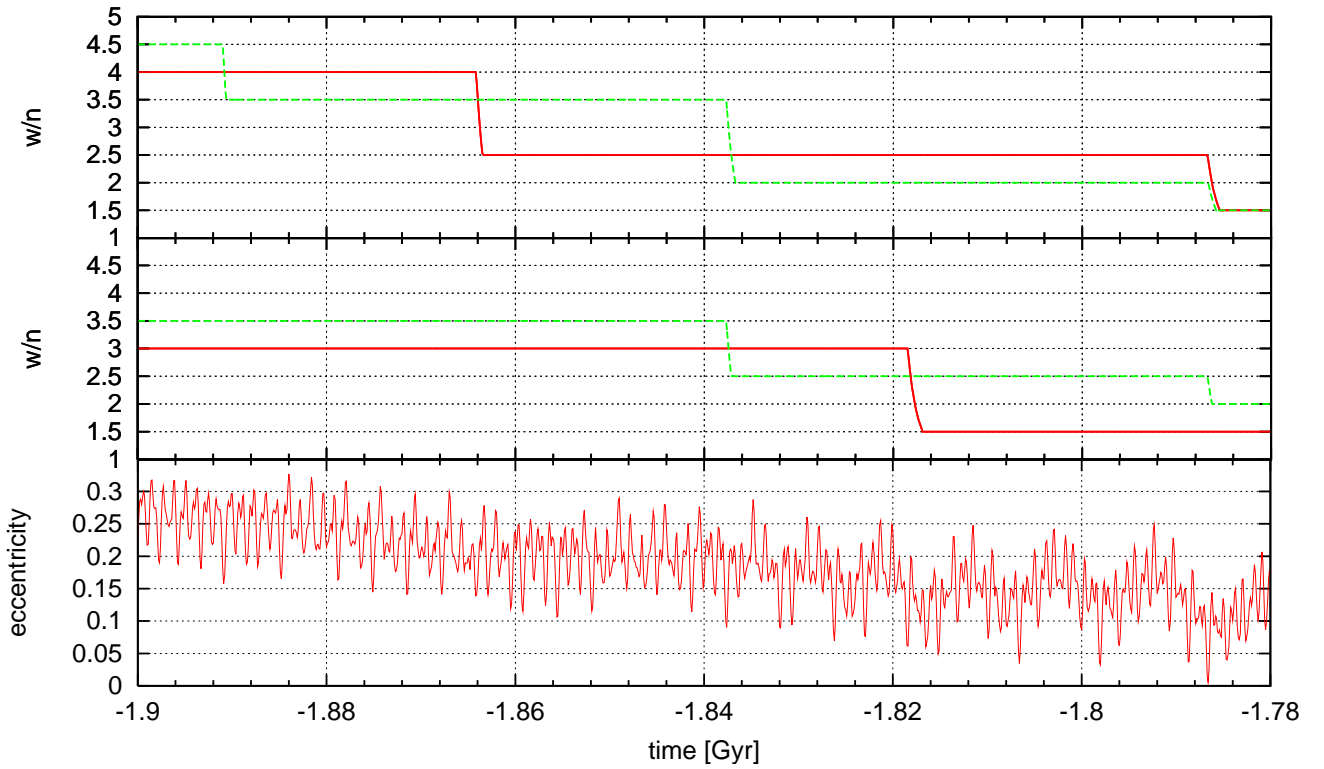


Figure 7: Four possible final evolutions for the spin of Mercury. Adopting a particular orbital solution, which presents a gradual decrease in the eccentricity (Fig.3a), we integrate close initial conditions for the spin. We observe that spin-orbit resonances are quit immediately after the eccentricity is below the critical values listed in Table 2. After being destabilized, the spin can evolve directly to the present 3/2 configuration, or can be trapped in an intermediate spin-orbit resonance. We purposely left one situation where the spin does not end in the 3/2 resonance. At the moment the eccentricity becomes lower than  $e_{2/1} \approx 0.0046$ , the spin is still captured in the 5/2 resonance. This resonance is then destabilized, but when the spin encounters the 2/1 resonance the eccentricity is already higher than  $e_{2/1}$ . Thus, there is a chance of capture in this resonance, preventing a subsequent evolution toward the 3/2 state.

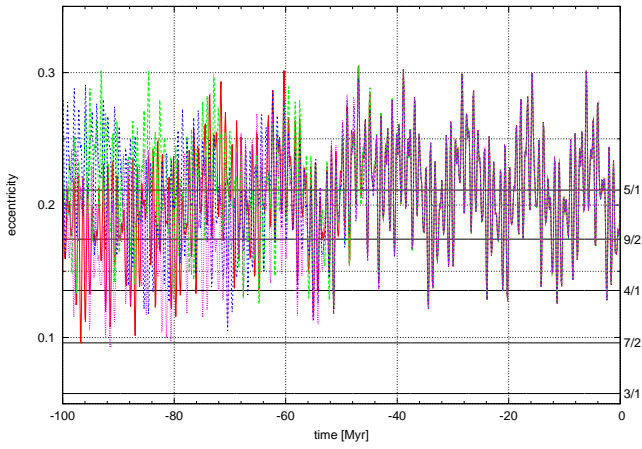


Figure 5: Some examples of the recent evolution of the eccentricity of Mercury. During the last 50-60 Myr all the orbits present the same evolution, before which the chaos effect takes place. Horizontal lines correspond to the critical eccentricities that destabilize the equilibrium in a given spin-orbit resonance (Tab.2). During the last 50 Myr the eccentricity was certainly below 0.13, thus the 4/1 resonance is not a possible final outcome for Mercury. For some orbits the eccentricity is below 0.09 in the last 100 Myr and the 7/2 resonance was also destabilized. However, since this scenario is not true for all orbital solutions, we may expect a few final evolutions captured in this last configuration (Tab.4).

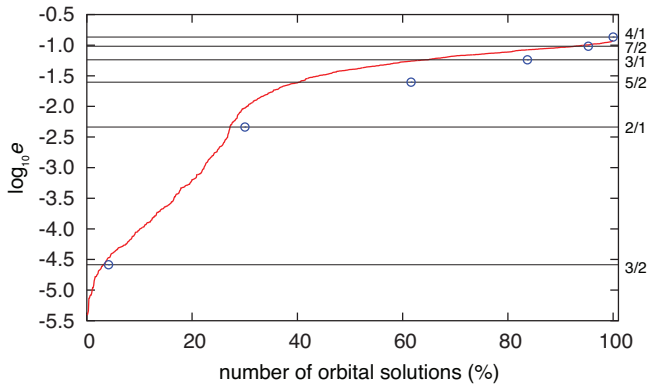


Figure 6: Cumulative distribution of the minimal eccentricities attained for the 1000 orbital solutions that we used. Straight lines represent the critical values of the eccentricity for each spin-orbit resonance (Tab.2), while dots represent the amount of captures obtained numerically for spin-orbit resonances that are still stable below each critical value of the eccentricity (Tab.4).